Journal of Solid State Chemistry 183 (2010) 2358–2364

Contents lists available at ScienceDirect

Journal of Solid State Chemistry

journal homepage: www.elsevier.com/locate/jssc

Cetyltrimethylammonium bromide assisted self-assembly of $NiTe_2$ nanoflakes: Nanoflake arrays and their photoluminescence properties

Ling Jiang [a], Ying-Jie Zhu [a,*], Jing-Biao Cui [b]

[a] State Key Laboratory of High Performance Ceramics and Superfine Microstructure, Shanghai Institute of Ceramics, Chinese Academy of Sciences, Shanghai 200050, PR China
[b] Department of Physics and Astronomy, University of Arkansas at Little Rock, Little Rock, AR 72204, USA

ARTICLE INFO

Article history:
Received 15 May 2010
Accepted 3 August 2010
Available online 6 August 2010

Keywords:
$NiTe_2$
Nanoflake
Array
Self-assembly
Photoluminescence

ABSTRACT

$NiTe_2$ nanoflakes and their self-assembled nanoflake arrays (one-dimensional nanostructures) have been prepared by a single-step hydrothermal method using $Ni(CH_3COO)_2 \cdot 4H_2O$, Na_2TeO_3, glucose, and cetyltrimethylammonium bromide (CTAB). CTAB was found to strongly influence the structure and morphology of the resultant $NiTe_2$. Morphological transformations from nanoflakes to self-assembled nanoflake arrays and then to solid smooth nanowires were observed as CTAB concentration was increased in the growth solution. Photoluminescence of the $NiTe_2$ self-assembled nanoflake arrays was investigated for the first time and the formation mechanism of the $NiTe_2$ nanostructures is also discussed.

1. Introduction

Fabrication of nanostructures with controllable size and shape has been of great scientific and technological interest in the past decades. One-dimensional (1-D) nanostructures such as nanotubes and nanowires/nanorods have attracted much research attention due to their unique properties arising from their small sizes, large surface areas, quantum confinement effects, and dimensionality-dependent anisotropy [1].

Among various 1-D nanostructures, semiconducting tellurides with potential applications in thermoelectric and optoelectronic devices are being actively investigated. As one of the most important thermoelectric semiconductors, for example, PbTe and its alloys possessed a high Seebeck coefficient, low thermal conductivity, and high electric conductivity, making them attractive for refrigeration and generating electrical power from heat [2,3]. Theoretical investigations [4] suggested that Bi_2Te_3 nanowires may exhibit ZT values much larger than 1.0, resulting from both the enhanced thermoelectric power and electrical conductivity and the reduced thermal conductivity. This ZT value is significantly larger than that of bulk materials [5]. Cadmium telluride (CdTe) is a near-infrared band gap semiconductor (E_g=1.56 eV, 300 K) with novel optical and electrical properties. It has been widely used for a variety of applications, including photovoltaic devices [6], light emitting diodes [7], biological sensors [8], and nanoscale electronics [9]. Although many 1-D nanostructures of metal tellurides have been intensively investigated, only a few studies on nickel telluride ($NiTe_2$) nanostructures have been reported up to now. Li et al. [10] prepared $NiTe_2$ and $NiSe_2$ nanorods by a solvothermal method using the reaction of $NiCl_2 \cdot 2H_2O$ with tellurium and selenium in ethylenediamine. Peng et al. [11] reported the synthesis of CoTe and NiTe nanoclustered wires through a co-reduction method using $N_2H_4 \cdot H_2O$ as a reducing agent. Liu et al. [12] obtained hexagonal $NiTe_2$ nanoplates through an ethylenediamine tetraacetic acid (EDTA)-assisted solution route. Two-step Te template-directed synthesis was one of the most popular strategies for the fabrication of 1-D telluride nanostructures [13–16]. As a common reducing agent for the synthesis of tellurides [11,13–20], $N_2H_4 \cdot H_2O$ is hazardous to the environment.

In this article, we report on a simple, single-step, and less hazardous hydrothermal route to the synthesis of $NiTe_2$ nanoflakes and their self-assembled nanoflake 1-D arrays. In addition, photoluminescence (PL) properties of the as-prepared $NiTe_2$ nanostructures were investigated and their origin is suggested. Possible formation mechanisms of the $NiTe_2$ nanostructures are discussed.

2. Experimental section

2.1. Chemicals

$Ni(CH_3COO)_2 \cdot 4H_2O$, Na_2TeO_3, glucose, and cetyltrimethylammonium bromide (CTAB) were purchased and used as received without further purification.

* Corresponding author. Fax: +86 21 52413122.
E-mail address: y.j.zhu@mail.sic.ac.cn (Y.-J. Zhu).

0022-4596/$ - see front matter © 2010 Elsevier Inc. All rights reserved.
doi:10.1016/j.jssc.2010.08.004

2.2. Synthesis of $NiTe_2$ 1-D nanostructures

In a typical procedure for fabrication of $NiTe_2$ nanostructures, different amounts of CTAB (0, 0.5, 1.5, 2.5, 3.5, and 5 g) were dissolved in 50 ml of deionized water; subsequently, $Ni(CH_3COO)_2 \cdot 4H_2O$ (0.248 g) was added to the above solution under magnetic stirring at room temperature. Afterwards 0.22 g of Na_2TeO_3 was added to the solution, and a green precipitate appeared immediately. After stirring for about 10 min, 3 g of glucose was added and then the mixture was stirred for 20 min to form a well-dispersed suspension. The mixture was put into a Teflon-lined stainless steel autoclave of 100 ml capacity and was sealed and heated at 160 °C for 12 h. After heating, the autoclave was cooled to room temperature in air naturally. The black products were collected by centrifugation, washed with deionized water and absolute ethanol several times, and then dried at 60 °C in vacuum.

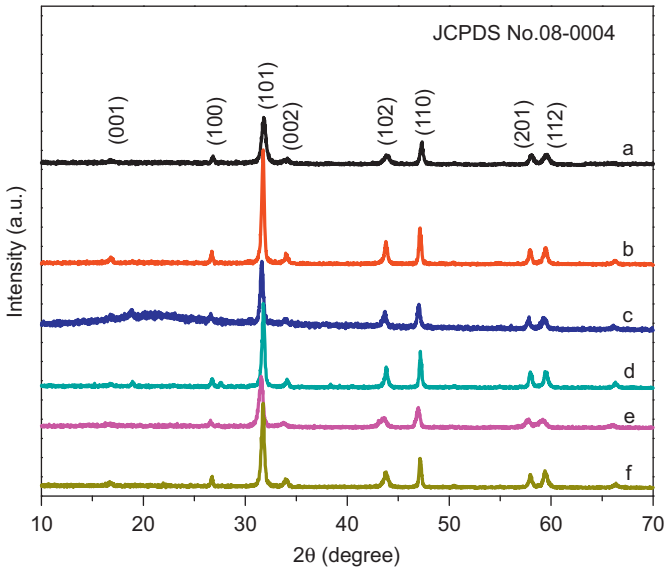

Fig. 1. XRD patterns of $NiTe_2$ samples synthesized with different amounts of CTAB in the growth solution: (a) 0 g, (b) 0.5 g, (c) 1.5 g, (d) 2.5 g, (e) 3.5 g, and (f) 5 g.

2.3. Characterizations

X-ray powder diffraction (XRD) patterns were recorded with a Rigaku D/MAX 2550V X-ray diffractometer with Cu $K\alpha$ radiation ($\lambda = 1.54178$ Å) and a graphite monochromator. Transmission electron microscopy (TEM) and high-resolution TEM (HRTEM) were performed with a JEOL JEM-2100F field-emission transmission electron microscope. Room-temperature photoluminescence was excited by the 325 nm line of a He–Cd laser. The emission light was focused onto the entrance of a monochromator and recorded by a CCD detector.

3. Results and discussion

3.1. Sample characterization and effects of CTAB

In order to investigate the effects of cetyltrimethylammonium bromide (CTAB) on morphology of the $NiTe_2$ nanostructures, controlled experiments were carried out by adjusting the

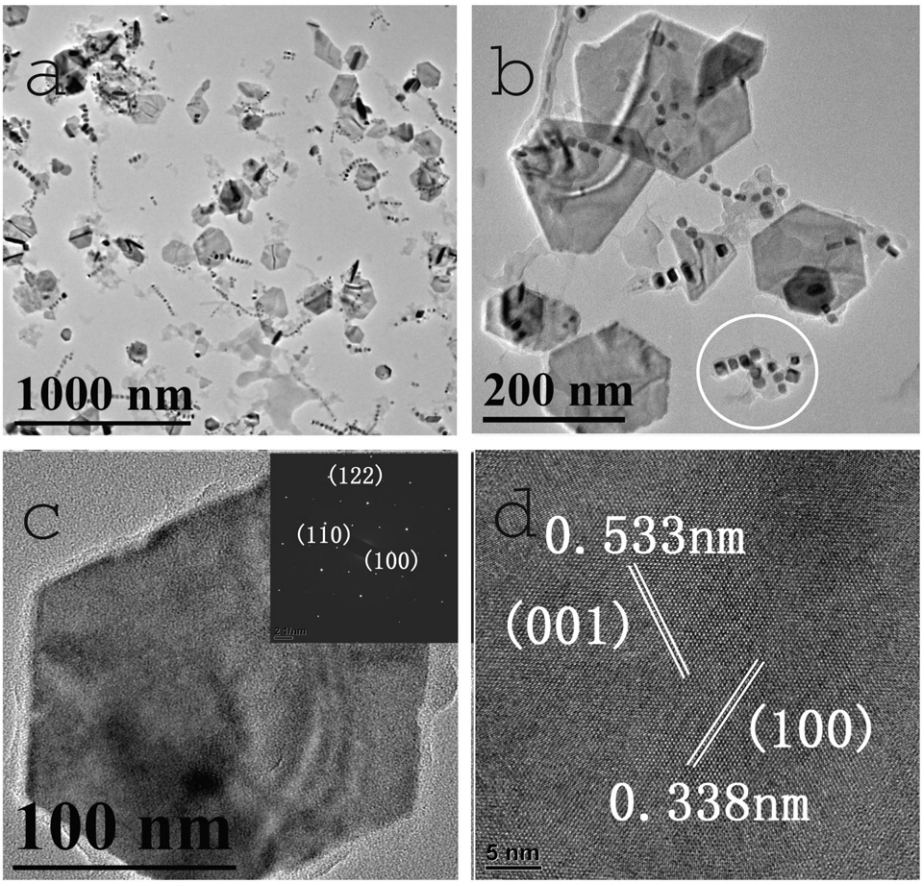

Fig. 2. TEM micrographs (a)–(c), SAED pattern (inset of (c)), and HRTEM image (d) of sample A prepared without CTAB.

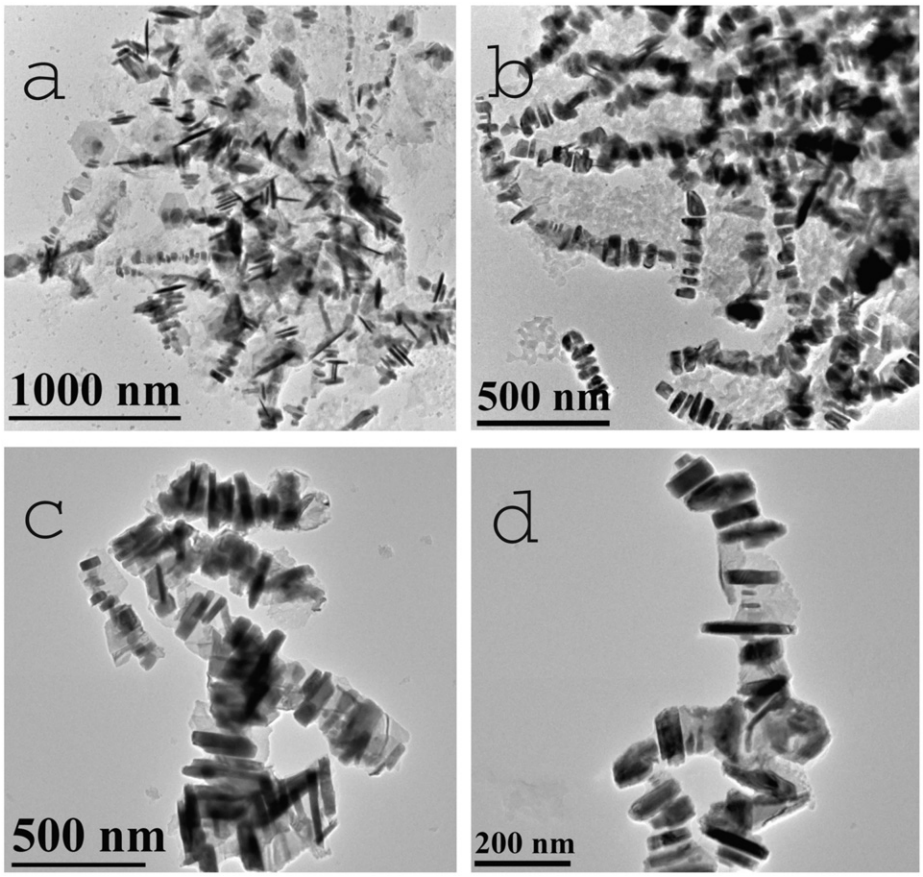

Fig. 3. TEM micrographs of sample B (0.5 g CTAB).

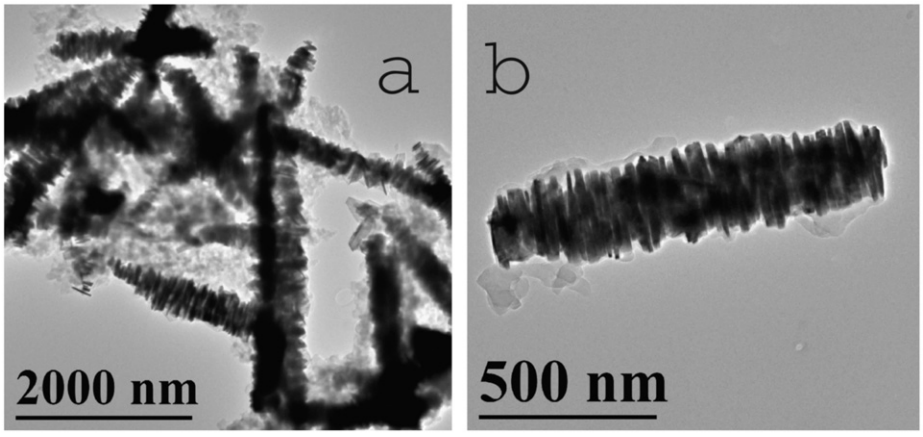

Fig. 4. TEM micrographs of sample C (1.5 g CTAB).

concentration of CTAB in the growth solution. Samples obtained with different amounts of CTAB are labeled as samples A (0 g CTAB), B (0.5 g CTAB), C (1.5 g CTAB), D (2.5 g CTAB), E (3.5 g CTAB), and F (5 g CTAB). Fig. 1 shows typical XRD patterns of the as-synthesized $NiTe_2$ nanostructures. The samples prepared with different amounts of CTAB have similar XRD patterns. All the diffraction peaks can be indexed to a single phase of $NiTe_2$ with a hexagonal crystal structure (JCPDS No. 08-0004).

Transmission electron microscopy (TEM) and high-resolution TEM (HRTEM) micrographs taken on the as-prepared $NiTe_2$ sample A are shown in Fig. 2. Nanoflakes of varied sizes from tens to hundreds of nanometers were observed. A magnified TEM image of sample A is shown in Fig. 2b, from which one can see that the nanoflakes are hexagonally shaped, thin nanoplates. Some ultra-small nanocrystals with sizes of around 15 nm, as highlighted by a circle in Fig. 2b, are also observed in the TEM image. These small nanocrystals are $NiTe_2$ nuclei, which would grow to the hexagonally shaped nanoflakes provided that the growth time is long enough. A typical individual hexagonal nanoflake of around 150 nm is displayed in Fig. 2c. Selected area electron diffraction (SAED) pattern was obtained for this nanoflake and is shown in the inset of Fig. 2c, revealing a single-crystalline structure of the nanoflake. This observation was further confirmed by the HRTEM image shown in Fig. 2d. The

measured *d*-spacing values for (0 0 1) and (1 1 0) planes are, respectively, 0.533 and 0.338 nm, which are consistent with the XRD results.

Addition of CTAB in the growth solution significantly affects the morphology of $NiTe_2$ nanostructures. Fig. 3 displays the TEM micrographs of sample B prepared with 0.5 g CTAB. Compared with sample A grown without CTAB, sample B has distinctive morphologies. As can be seen from Fig. 3, nanoflake arrays with lengths ranging from several hundred nanometers to a few micrometers are observed. These 1-D nanostructures are self-assembled arrays of the $NiTe_2$ nanoflakes with thicknesses of about 20–40 nm. However, the nanoflakes are not closely packed, exhibiting large spaces of tens of nanometers between the building blocks. In addition, the nanoflakes are not well aligned, which leads to a low degree of order of the 1-D nanostructures.

CTAB in the growth solution affected the organization of the $NiTe_2$ nanoflakes into self-assembled 1-D nanoflake arrays. In order to further investigate the key role played by CTAB in the formation of $NiTe_2$ nanostructures, samples were grown with increased amounts of CTAB. A close relationship between the amount of CTAB and the morphology of the self-assembled 1-D nanostructures was observed. Fig. 4 shows the TEM images of sample C prepared with 1.5 g CTAB. The nanoflakes are well assembled into 1-D nanoflake arrays. Both the compactness of the assembled nanoflakes and the degree of order are improved as compared with sample B prepared with 0.5 g CTAB. As shown in Figs. 5 and 6, similar results were obtained for sample D (2.5 g CTAB) and sample E (3.5 g CTAB), indicating that higher concentrations of CTAB help produce $NiTe_2$ 1-D nanoflake arrays with well-organized and closely packed nanoflakes.

Further increase of CTAB up to 5 g results in an interesting phenomenon, as shown in Fig. 7 for sample F. The average length of the $NiTe_2$ self-assembled 1-D nanoflake arrays increases as compared with the samples prepared with less CTAB. In addition, 1-D solid nanowires with diameters of about 100–200 nm and relatively smooth surfaces were observed. The SAED patterns taken on the typical 1-D nanoflake array and a single solid nanowire are, respectively, shown in Fig. 7c and d for comparison. The diffraction spots in the SAED pattern of Fig. 7c reveal that the nanoflakes in the 1-D nanoflake array are preferentially oriented although they are not in a perfect order of arrangement. In contrast, the SAED pattern taken on the single solid smooth nanowire is essentially composed of well-defined sharp dots, suggesting a single-crystalline structure of the nanowire. However, some defects in the solid smooth nanowire are visible in Fig. 7d. These defect lines are approximately perpendicular to the axis of the nanowire, implying that the nanowire is likely formed due to the transformation of 1-D nanoflake arrays into solid nanowire structures.

3.2. *Photoluminescence of self-assembled $NiTe_2$ 1-D nanoflake arrays*

To the best of our knowledge, there has been no report regarding optical properties of self-assembled $NiTe_2$ 1-D nanoflake arrays. In this study, their photoluminescence was measured at room temperature and is shown in Fig. 8. One can see from the PL spectrum that a broad emission band around 535 nm was observed. In general, it is hard to observe PL from transition-metal tellurides like $NiTe_2$ due to magnetic interactions, which quench

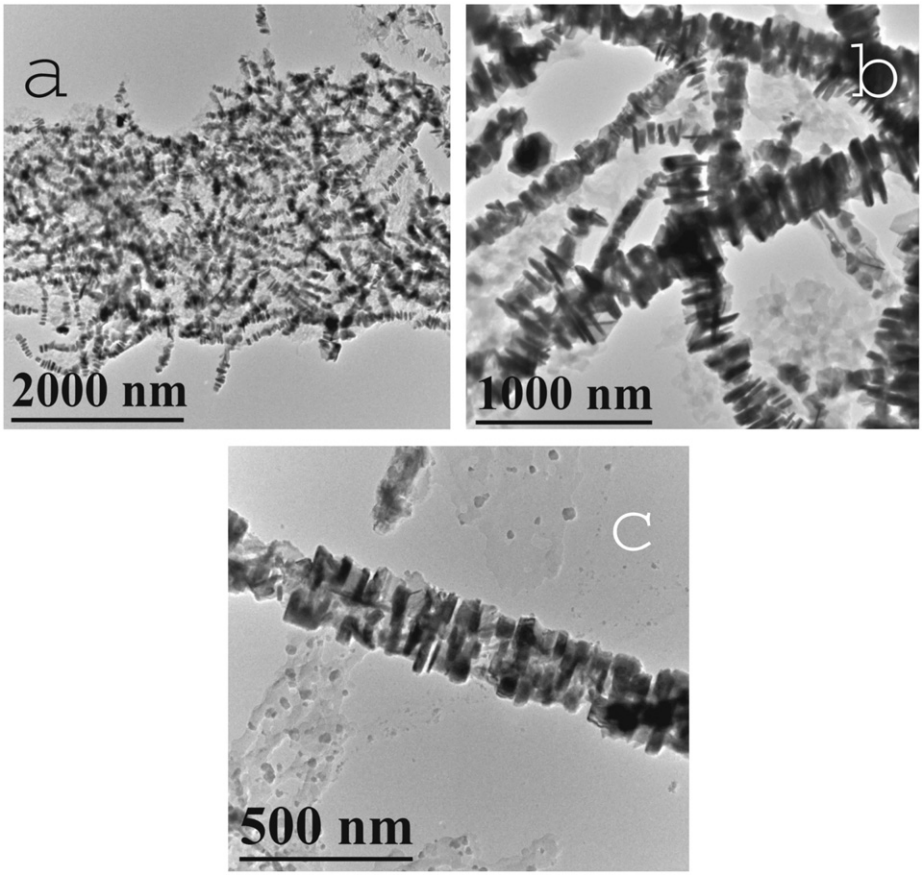

Fig. 5. TEM micrographs of sample D (2.5 g CTAB).

optical radiation. Nonetheless, the optical properties of tellurides may dramatically change when their size is reduced down to the nanometer scale. Quantum confinement and surface effects become prominent with such small dimensions. Quantum confinement effects may induce delocalized states and enhance the electron–phonon interaction, leading to optical transitions in the nanostructures that are not present in bulk materials. Reduction of magnetic interaction also occurs on the nanometer scale and results in the formation of nonmagnetic covalent bonds, especially on surfaces of the nanostructures. In addition, a large amount of surface states, defects, dangling bonds, and tiny clusters are also present on the surfaces. The observed PL in the self-assembled $NiTe_2$ 1-D nanoflake arrays may result from a combination of these effects at the extremely small size. The very broad emission band seems to suggest that surface states and defects could be majorly responsible for the observed PL. Broad band emissions from other telluride nanomaterials were also reported in the literature. For example, very small CdTe nanoclusters at the initial growth stage exhibit a broad defect emission band, which is replaced by an exitonic emission as the crystal size increases [21]. This observation further supports that the surface states and defects may cause the broad band emissions of $NiTe_2$ nanostructures. Further investigations are still needed to fully understand the PL mechanism.

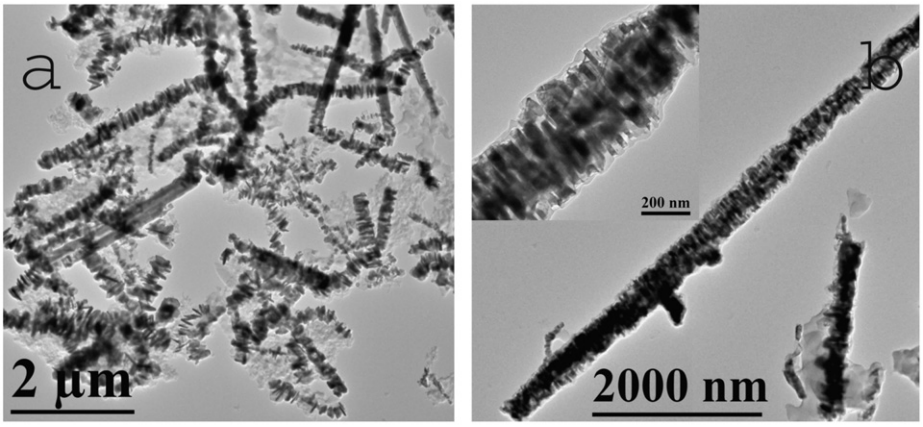

Fig. 6. TEM micrographs of sample E (3.5 g CTAB).

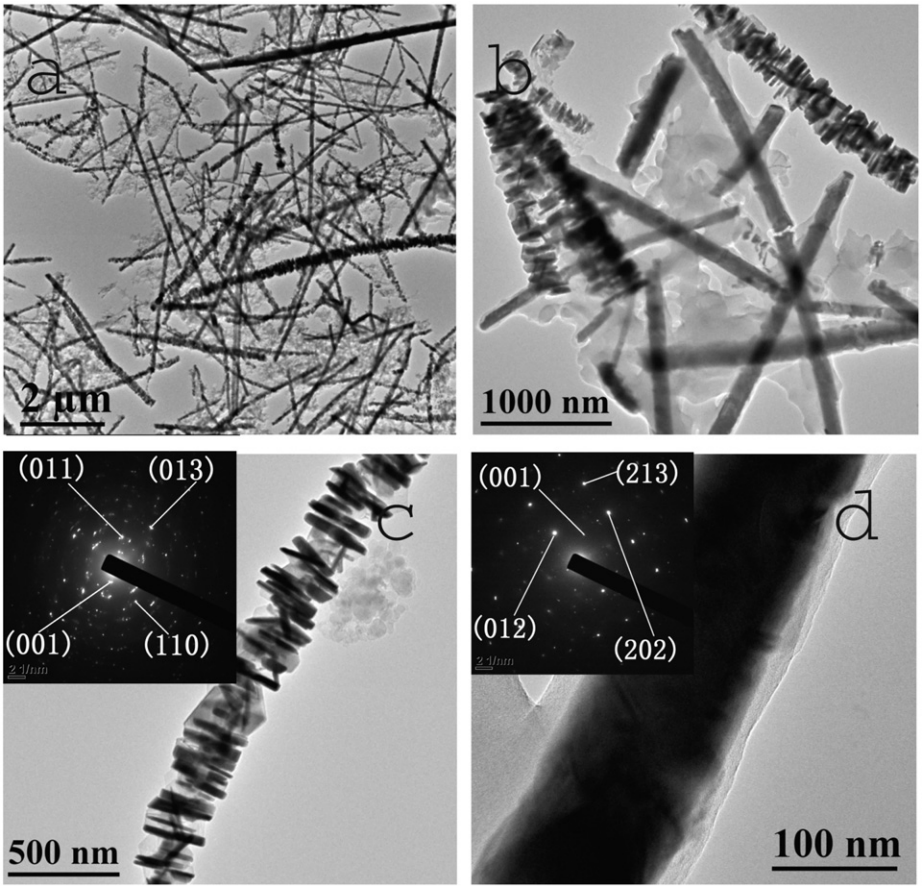

Fig. 7. TEM micrographs (a)–(d) and SAED patterns (insets of (c) and (d)) of sample F (5 g CTAB).

3.3. Possible reaction process

It is known that glucose is a weak reducing agent due to the presence of the aldehyde group [22], which can be easily oxidized to carboxyl under hydrothermal conditions. Glucose may slowly reduce Te^{4+} to Te^{2-} in solutions at certain temperatures. For example, Fan et al. [23] reported a glucose-assisted solution route to the synthesis of CoTe nanotubes, in which glucose functioned as a reducing agent to reduce TeO_2 to Te^{2-} at high temperature. During the hydrothermal preparation of Ag_2Te–Ag composites performed by Batabyal and Vittal [24], glucose was also used as an agent to reduce TeO_3^{2-} to Te^{2-}. Here we propose a possible reaction process for the formation of $NiTe_2$ hierarchical 1-D nanostructures due to self-assembly of $NiTe_2$ nanoflakes. The glucose assisted chemical reduction is given as follows:

$$C_5H_{11}O_5CHO + TeO_3^{2-} \xrightarrow{160\,^{\circ}C} Te^{2-} + C_5H_{11}O_5COOH + O_2\uparrow$$

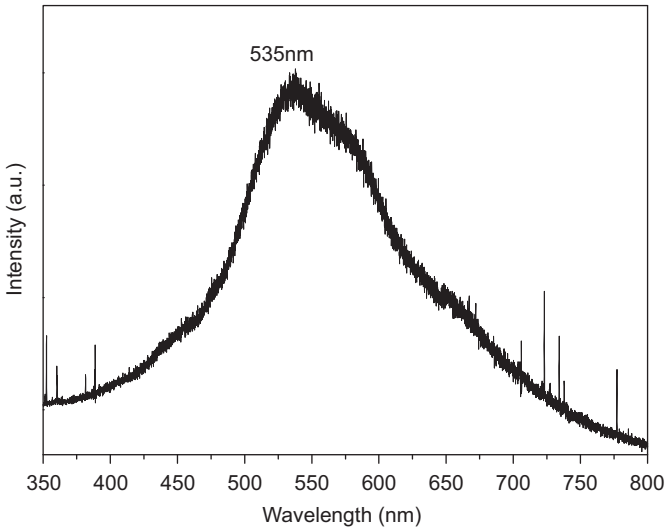

Fig. 8. Room temperature photoluminescence spectrum of self-assembled $NiTe_2$ 1-D nanoflake arrays (sample C).

3.4. Possible formation mechanism

The formation mechanism of $NiTe_2$ self-assembled nanoflake arrays is shown in Fig. 9. In the early stage, soluble Na_2TeO_3 is dissociated into TeO_3^{2-} and Na^+ ions in water, and then TeO_3^{2-} reacts with Ni^{2+} to form $NiTeO_3$ precipitate, which is insoluble in water at room temperature. When the mixed reaction reagents are hydrothermally heated at a higher temperature such as 160 °C, $NiTeO_3$ precipitate begins to dissolve. As a weak reducing agent, glucose can slowly reduce Te^{4+} to Te^{2-} in solution. The combination of Te^{2-} and Ni^{2+} results in the formation of $NiTe_2$ nuclei, and these nuclei grow to $NiTe_2$ nanoflakes with hexagonal morphologies.

As a commonly used surfactant, CTAB has been widely applied in preparing nanowires because it can form a rodlike micellar structure to assist in the formation of nanowires and nanorods [25]. The concentration of CTAB is an important factor that determines the morphology of the product. This speculation has been experimentally demonstrated in this work. Referring to Fig. 9, we propose the formation process of $NiTe_2$ self-assembled 1-D nanoflake arrays as follows. (1) Firstly, CTAB molecules were adsorbed onto the surfaces of the newly formed $NiTe_2$ nanoflakes. The surface-bound CTAB molecules provide steric as well as electrostatic repulsion between nanocrystals when they approach each other in solution [26]. (2) These interactions help adjacent nanoflakes to find a better coordination among them through relative rotation and therefore result in the formation of aligned arrays of nanoflakes by self-assembly under hydrothermal conditions. According to the previous reports by Sau and Murphy [26] and Jana et al. [27], on solvent evaporation, these CTAB molecules can paradoxically assist in drawing the vertical nanoflakes closer by sharing a common layer of counterions or through the interdigitation of CTAB tails from neighboring nanoflakes. These reported data support our explanations for the formation of $NiTe_2$ self-assembled 1-D nanoflake arrays. (3) The growth mode for $NiTe_2$ solid smooth nanowires may be explained as follows. Under a higher concentration of CTAB, the nanoflakes are closely packed 1-D nanostructures with relatively small spaces between the nanoflakes. Further growth of the nanoflakes along the axial direction of 1-D nanoflake arrays causes them to fuse with each other and form solid nanowires under hydrothermal conditions. Note that the average diameter of solid nanowires is smaller than that of 1-D nanoflake arrays and the nanowire surfaces are smooth. We propose that the dissolution along

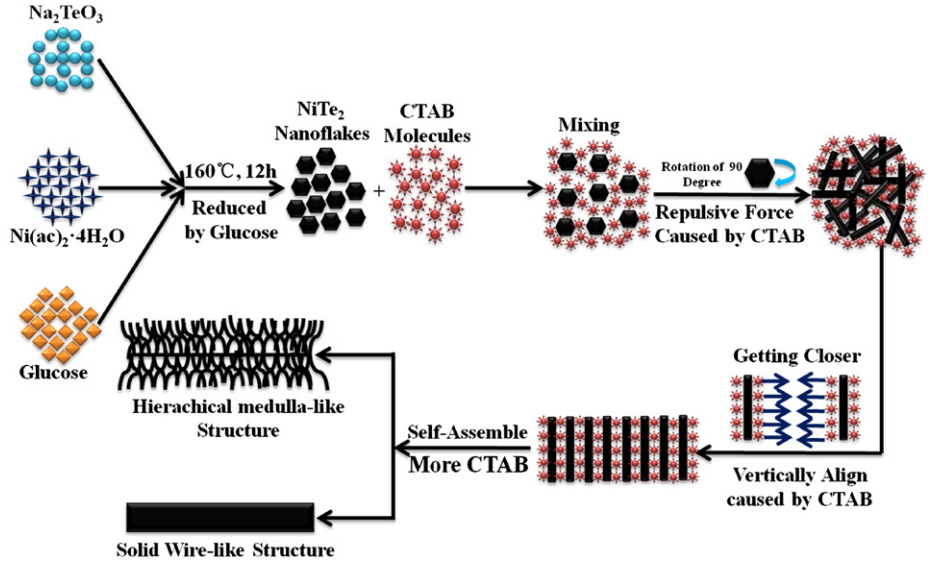

Fig. 9. Illustration for the formation mechanism of $NiTe_2$ nanoflakes and self-assembled $NiTe_2$ 1-D nanoflake arrays synthesized with different amounts of CTAB.

the radial direction smoothens the nanowire surface in contrast with the fusion of nanoflakes due to axial growth. The materials dissolved along the radial direction will in turn help the local axial growth, leading to the merging of adjacent nanoflakes and reduction of diameter of the nanowires. Note that the growth rate along the axes of the nanoflake arrays is low. Therefore, the $NiTe_2$ solid smooth nanowires can be observed only with high CTAB concentrations, under which spaces between the nanoflakes in the 1-D nanostructures are so small that they can be easily filled by further growth.

4. Conclusion

In summary, we have developed a facile hydrothermal route to the synthesis of $NiTe_2$ nanoflakes and self-assembled $NiTe_2$ 1-D nanoflake arrays using $Ni(CH_3COO)_2 \cdot 4H_2O$, Na_2TeO_3, glucose, and cetyltrimethylammonium bromide (CTAB). It was found that CTAB had a significant influence on structure and morphology of the $NiTe_2$ nanostructures. Morphological transformations from nanoflakes to self-assembled $NiTe_2$ 1-D nanoflake arrays and then to solid smooth nanowires were realized with the assistance of CTAB. Photoluminescence properties of the self-assembled $NiTe_2$ 1-D nanoflake arrays were investigated. A broad PL emission centered at 535 nm was observed, which is explained in terms of surface states and defects at the nanometer scale. The formation mechanism of the $NiTe_2$ nanostructures was also proposed.

Acknowledgments

This work is financially supported by the National Natural Science Foundation of China (50772124, 50821004), and the Opening Project of State Key Laboratory of High Performance Ceramics and Superfine Microstructure (SKL200901SIC).

References

[1] A.P. Alivisatos, Science 271 (1996) 933.
[2] T.M. Tritt, Science 283 (1999) 804.
[3] K.F. Hsu, S. Loo, F. Guo, W. Chen, J.S. Dyck, C. Uher, T. Hogan, E.K. Polychroniadis, M.G. Kanatzidis, Science 303 (2004) 818.
[4] M.S. Dresselhaus, G. Dresselhaus, X. Sun, Z. Zhang, S.B. Cronin, T. Koga, J.Y. Ying, G. Chen, Microscale Therm. Eng. 3 (1999) 89.
[5] J. Ham, W. Shim, D.H. Kim, S. Lee, J. Roh, S.W. Sohn, K.H. Oh, P.W. Voorhees, W. Lee, Nano Lett. 9 (2009) 2867.
[6] I. Gur, N.A. Fromer, M.L. Geier, A.P. Alivisatos, Science 310 (2005) 462.
[7] N.P. Gaponik, D.V. Talapin, A.L. Rogach, A. Eychmuller, J. Mater. Chem. 10 (2000) 2163.
[8] S.P. Wang, N. Mamedova, N.A. Kotov, W. Chen, J. Studer, Nano Lett. 2 (2002) 817.
[9] P.E. Trudeau, M. Sheldon, V. Altoe, A.P. Alivisatos, Nano Lett. 8 (2008) 1936.
[10] B. Li, Y. Xie, J.X. Huang, H.L. Su, Y. Qian, Nanostruct. Mater. 11 (1999) 1067.
[11] Q. Peng, Y.J. Dong, Y.D. Li, Inorg. Chem. 42 (2003) 2174.
[12] X.Y. Liu, R.Z. Hu, L.L. Chai, H.B. Li, J. Gu, Y.T. Qian, J. Nanosci. Nanotechnol. 9 (2009) 2715.
[13] H.W. Liang, S. Liu, Q.S. Wu, S.H. Yu, Inorg. Chem. 48 (2009) 4927.
[14] G.A. Tai, W.L. Guo, Z.H. Zhang, Cryst. Growth Des. 8 (2008) 3878.
[15] P.F. Zuo, S.Y. Zhang, B.K. Jin, Y.P. Tian, J.X. Yang, J. Phys. Chem. C 112 (2008) 14825.
[16] G. Tai, B. Zhou, W.L. Guo, J. Phys. Chem. C 112 (2008) 11314.
[17] P. Kumar, K. Singh, Cryst. Growth Des. 9 (2009) 3089.
[18] F.Y. Li, C.G. Hu, Y.F. Xiong, B.Y. Wan, W. Yan, M.C. Zhang, J. Phys. Chem. C 112 (2008) 16130.
[19] H. Gong, X.P. Hao, C. Gao, Y.Z. Wu, J. Du, X.G. Xu, M.H. Jiang, Nanotechnology 19 (2008) 445603.
[20] A.M. Qin, Y.P. Fang, P.F. Tao, J.Y. Zhang, C.Y. Su, Inorg. Chem. 46 (2007) 7403.
[21] S.F. Wuister, F. van Driel, A. Meijerink, J. Lumin. 102 (2003) 327.
[22] Y.M. Sui, W.Y. Fu, H.B. Yang, Y. Zeng, Y.Y. Zhang, Q. Zhao, Y.G. Li, X.M. Zhou, Y. Leng, M.H. Li, G.T. Zou, Cryst. Growth Des. 10 (2010) 99.
[23] H. Fan, Y.G. Zhang, M.F. Zhang, X.Y. Wang, Y.T. Qian, Cryst. Growth Des. 8 (2008) 2838.
[24] S.K. Batabyal, J.J. Vittal, Chem. Mater. 20 (2008) 5845.
[25] X.C. Song, Y. Zhao, E. Yang, Y.F. Zheng, L.Z. Chen, F.M. Fu, Cryst. Growth Des. 9 (2009) 344.
[26] T.K. Sau, C.J. Murphy, Langmuir 21 (2005) 2923.
[27] N.R. Jana, L.A. Gearheart, S.O. Obare, C.J. Johnson, K.J. Edler, S. Mann, C.J. Murphy, J. Mater. Chem. 12 (2002) 2909.